RESEARCH PAPER

Synthesis and Characterization CuO-ZnO Binary Nanoparticles

*Adnan M. Mansoor Al-Saeedi [1], Firas K. Mohamad [1] and Noor J. Ridha [2]**

[1] Deartment of Environmental Health, College of Applied Medical Sciences, University of Kerbala, Iraq

[2] Department of Physics, College of Science, University of Kerbala, Kerbala, Iraq

ARTICLE INFO

Article History:
Received 03 February 2022
Accepted 12 June 2022
Published 01 July 2022

Keywords:
CuO-ZnO
Hydrothermal
Nanostructures
XPS

ABSTRACT

In this work, a simple and low cost modified hydrothermal method was used to prepare CuO-ZnO nanostructures. The innovation of this work is to modify hydrothermal method by flowing nitrogen gas during the reaction. Structural, morphological, optical, and chemical species of grown crystals were studied using the techniques of X-ray diffraction (XRD), Scanning Electron Microscopy (SEM), high-resolution transmission electron microscopy HRTEM, x-ray photoelectron spectroscopy (XPS), UV/Vis spectroscopy and photoluminescence (PL). Specifically, XRD analysis shows that the sample has hexagonal structure with no phases of impurity indicating the Zn ions have been effectively integrated into the standard CuO crystal structure. The parameters of the lattice, the length of the unit cell and the crystallite size were determined from the XRD pattern of the CuO-ZnO sample and it was noticed that the crystallite size ranged from 17 nm to 26 nm. The SEM micrographs of the sample CuO-ZnO revealed that the prepared sample exhibited nanorods-like structure. The XPS spectrum proved the presence of Cu^{+2} and Zn^{+2} elemental forms. It is also observed that the XPS spectrum was free from other peaks related to impurities which indicating that the prepared sample was pure. The optical characterization recorded that the energy gap was around 2.51 eV while PL spectrum showed blue and red orange emissions originated from CuO-ZnO nanostructures.

How to cite this article
Mansoor Al-Saeedi A M., Mohamad F K., Ridha N J. Synthesis and Characterization CuO-ZnO Binary Nanoparticles. J Nanostruct, 2022; 12(3):686-696. DOI: 10.22052/JNS.2022.03.021

INTRODUCTION

Nanotechnology is one of the most promising field due to their large range of applications [1]. It is well known that the size of nanomaterials plays an effective role in controlling their properties owing to the quantum confinement effects. Besides, the morphology of nanomaterials is the most principal parameter that affects the surface area since it controls the fraction of the molecules existing on the surface. Therefore, meticulous efforts have been focused on developing materials in various morphologies such as nanospheres [2, 3], nanotubes [4, 5], core-shell [6] and nanorods [7-9] which exhibited high performance in several fields of applications.

Semiconductor nanomaterials have attracted extensive investigations from theoretical and experimental standpoints, due to their wide range of applications in environment and optoelectronic technological devices [10-13]. Their applications are well known in several areas such as antibacterial [14], solar cells [15], electrodes [16], gas sensing

* Corresponding Author Email: nooraboalhab@yaho.com

[17], photocatalytic [18-23], liquid crystal displays [24], etc.

The main attractive and critical property of the metal oxides semiconductors is their energy gap, hence it varied from wide to narrow depending on the type of metal oxide. Copper oxide (CuO) is a p-type semiconductor which has a narrow bandgap around 1.2 eV [25]. Earlier publications focused on the preparation of CuO using different methods such as sol-gel [26], hydrothermal [27], chemical vapor deposition (CVD) [28], pulsed laser deposition (PLD) [29], etc. Recently CuO was doped with several elements such as Al using sol-gel method [30], Au by wet chemistry method [31, 32], Ti by microwave method [33, 34] and so on.

Nowadays, designing a novel composite with promising properties is the crucial demand to enhance its performance. Binary system is the recent motivation for several researches, as example SnO_2-CuO binary system was synthesis by hydrothermal method [35, 36]. As well, CuO-TiO_2 nanofluid was prepared by chemical method [37]. Nevertheless, Zinc oxide (ZnO) is one of the most interesting n-type semiconductor metal oxides because of the large direct bandgap (~3.37 eV at room temperature) which is applicable in various fields [38, 39]. Therefore, the creation of a binary system of CuO-ZnO provides new properties and therefore enhances their performance. Thus, CuO was as well doped with Zn using different preparation methods. For example, the co-precipitation method was used for doping ZnO by Cu ions in which hexagonal structure was obtained [40]. As well, another group of researchers studied the effects of different precursors [41]. Meanwhile, other researchers used solid-state method to prepare copper doped zinc oxide hence the achieved irregular structure with dimensions varied from 50 – 100 nm [42]. Recently, CuO was doped with Zn by electrodeposition method in which large particles size in the range of 1-10 µm were obtained by increasing Zn concentration [43].

In this work, CuO-ZnO nanorods were successfully prepared via a facile and economic modified hydrothermal method in which nitrogen (N_2) gas. The novelty of this work is purging N_2 gas to increase the surface area. The structural and optical properties were investigated in details.

MATERIALS AND METHODS

To prepare CuO-ZnO nanoparticles modified hydrothermal method was used. First, Copper chloride $CuCl_2$ from Sigma-Aldrich and zinc nitrate Zn $(NO_3)_2$ from PubChem was separately dissolved in 100 ml of DI water. Then, the two solutions were vigorously stirring to ensure the solution mixed well. Drops of NaOH (0.1 M) was gradually added to the solution to control the pH value (pH=11). The solution was poured into a reactor then heated at 90 ˚C for 3 h. The novelty of this work is to flow nitrogen gas during reaction thus porous structures could be obtained. The precipitation was washed with DI water, dried at 100 ˚C for 1 h and finely annealed at 300 ˚C for 1 h.

The prepared sample was characterized by several techniques in order to investigate its structural and optical properties. The purity was studied by X-ray diffractometer (XRD) from Cu Kα with λ=0·1518 nm via smart-lab. Hitachi (S-4800) scanning electron microscopy (SEM) and JEOL JEM-2100 transmission electron microscopy (TEM) were used to monitor the morphology. X-ray photoelectron spectroscopy (XPS). Ultraviolet/visible spectrometer (UV/Vis) model PE lambda 750S and FLS 1000 photoluminescence spectroscopy (PL) were used to investigate the optical properties. These characterizations with their explanations could provide informative investigations on the prepared CuO-ZnO binary nanoparticles.

RESULTS AND DISCUSSIONS

Typical X-ray diffraction (XRD) of the prepared sample CuO-ZnO is shown in Fig. 1. The sample exhibited a single-phase ZnO with a wurtzite hexagonal structure (space group P63mc) matching the standard diffraction pattern (JCPDS 01-079-0207). In general, the diffraction pattern showed three main peaks at 2Θ°= 31.7, 34.3 and 36.2 were corresponding to 100, 002 and 101 are related to ZnO. For ZnO, the preferred orientation was at (101) represented ZnO structures grown in a-direction while the growth in other orientations was retarded. The crystal size = 26.45 nm which was calculated according to (101) peak while a=b= 2.65Å and c= 4.9Å.

Whilst another two main peaks related to Cu were detected at 2Θ° = 35.62 and 38.68 were matched to (100) and (111). Hence the preferred orientation is at (100) an evident to the growth of CuO Tenorite Monoclinic structures (JCPDJ=01-072-0629). The lattice parameters a= 4.35 Å, b =3.254 Å and c= 4.98 Å and the average Crystallite Size =17.48 nm. It is also noticed from

the diffractograms, the presence of small peaks at 2Θ° = 17.63 and 41.58 which are related to other Cu components. These peaks matched 00-023-0954 (Cu_2O_2 Melanothallite Orthorhombic). This XRD pattern appeared lowest than other peaks which indicate the lowest ratio due to growth environments.

It is worth comparing the calculated lattice parameters of ZnO (a=b= 2.65Å and c= 4.9Å) with their corresponding theoretical values related to reference code (JCPDJ=01-079-0207) which equal to a=b=3.2568 Å and c= 5.2125Å. It is clear that there is a variation in these values in which the a and b become larger while c become smaller. This is in fact due to the disturbance of the presence of Cu hence the ionic radii of Cu = 140 pm and Zn= 139 pm.

It is valued to compare this work with previously reported work, as example the CuO-ZnO structures were prepared via microwave method [44]. The XRD reported results indicated the formation of hydrozincite and aurichalcite structures. While another group of researchers reported that the dominant structure in ZnO-CuO prepared sample was the hexagonal wurtzite with some Cu ions substitutional the Zn ions [45]. Nevertheless, the CuO-ZnO was synthesized previously and both wurtzite and monoclinic structures were obtained [46].

The field emission scanning electron microscope (FESEM) of sample CuO-ZnO is shown in Fig. 2. The prepared nanoparticles are agglomerated to reduce their surface energy. A closer view to Fig. 2(b) gives the sense that the prepared sample exhibited a rod-like structure. The estimated nanorods diameter is around 25-26 nm as shown in Fig. 2(d).

Fig. 3 shows the energy dispersive X-ray spectroscopy (EDX) of the prepared CuO-ZnO sample. The EDX analysis results illustrate that the prepared sample is composed of Cu, Zn and O. The atomic ratio of the elements is as follow; Zn=12.2%, Cu=37.12% and O=50.68%. By comparison the atomic percentage ratio of the ratio of Zn: Cu is around 1:3, indicated the majority amount of Cu element in the structure. Meanwhile, (Cu+Zn) :O is almost 1:1 with a slightly higher O ratio. This evidently supports that the prepared sample is CuO - ZnO nanostructures. Similar results were found elsewhere hence the O was higher that both Cu and Zn [47].

For further confirmation of the elemental composition and distribution, the EDX mapping was conducted as shown in Fig. 4. The survey scan proved the presence of Cu, Zn and O elements. These elements were distributed homogeneously and uniformly on the entire sample. It's clear that the highest ratio is for Cu and O elements as in Fig. 4(a and c). Nevertheless, the existence of the Zn element is lower and well distributed in the sample as in Fig. 4(b). No other elements were detected even in a very small ratio as in the

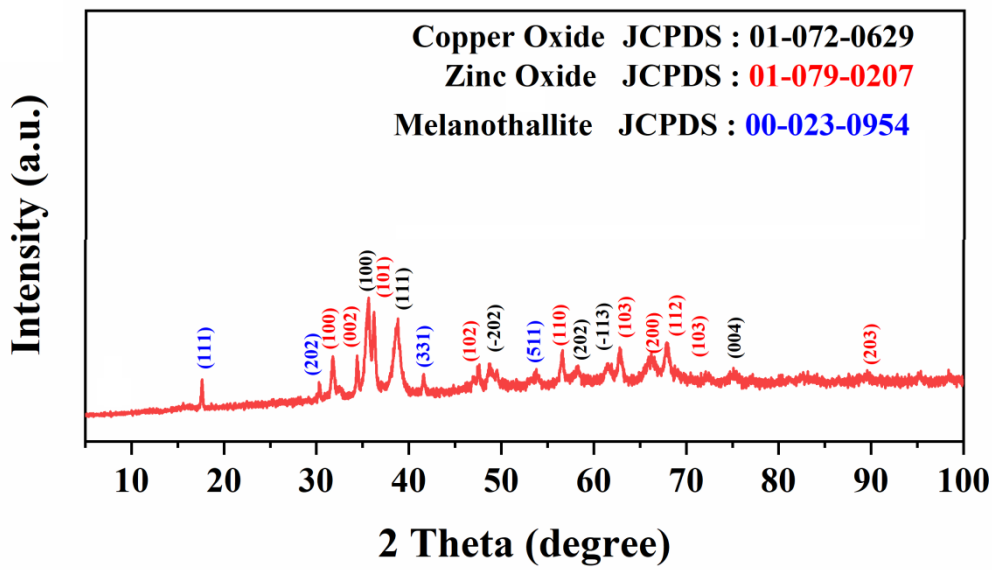

Fig. 1. XRD spectra of the prepared sample

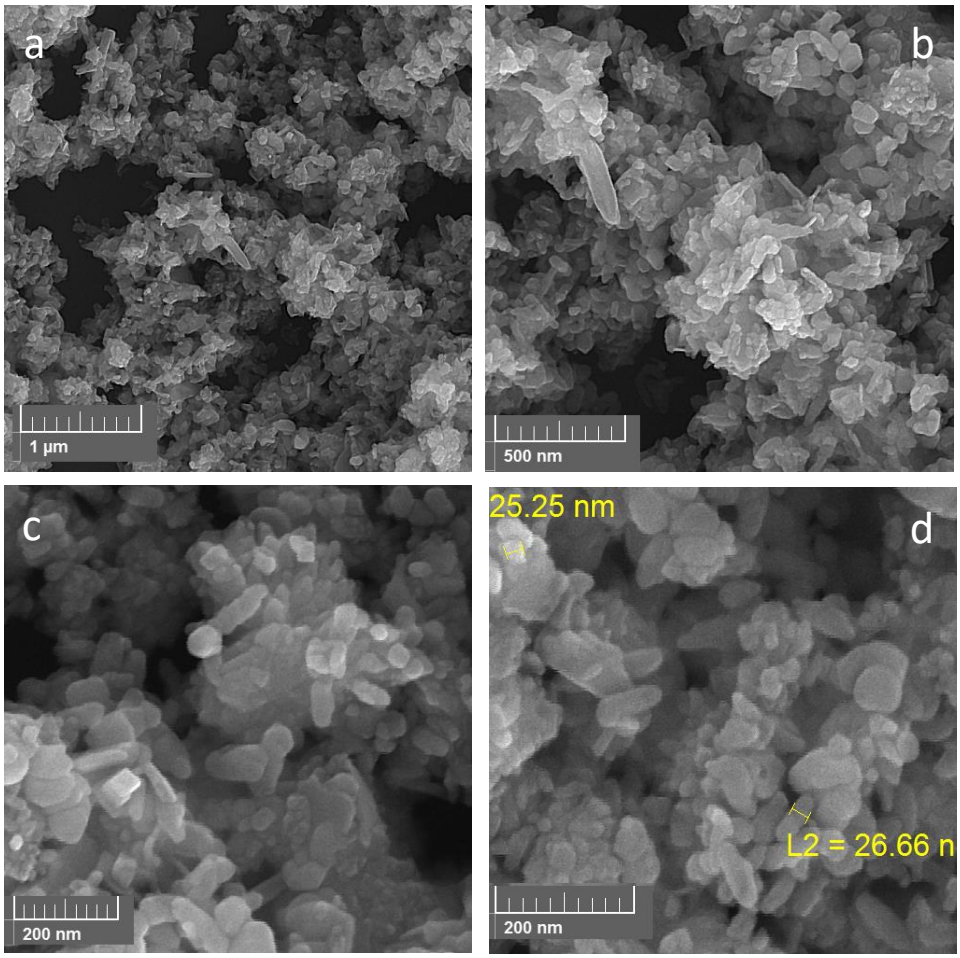

Fig. 2. FE-SEM micrographs of CuO-ZnO nanostructures at different magnification where (a) is the low magnification 35kX, (b) higher magnification 75 kX, (c) 150kX and (d) the highest 200kX.

figures. This could be attributed to the high quality of the preparation method. The presence of the elements in well-distributed form proved that the prepared sample is a composite of the Cu, O, and Zn.

The TEM, HRTEM and SAED of sample CuO-ZnO were investigated and are shown in Fig. 5. The wide range scan of TEM revealed the formation of rod-like nanoparticles as presented in Fig. 5(a). Higher magnification revealed that the length of the rods is 100 to 200 nm and the diameter 20-40 nm as shown in Fig. 5(b) which matching well the SEM results. High magnification TEM discovered the existence of quantum dots coating the rods as in Fig. 5 (c and d). The SAED prove the existence of monoclinic CuO patterns with rings of (111) and (100) as in Fig. 5(e). As well, the hexagonal ZnO structures were appeared as well represented with rings denoted by (100), (002), (101) and (102). The appearance of both phases related to CuO and ZnO indicated the formation of a composite material. The HRTEM showed the interplanar spacing d=0.274 nm related to the peak (110) of CuO monoclinic structure, as well, the d=0.282 nm corresponds to Hexagonal ZnO (100) as shown in Fig. 5(f). These results proved the presence of polycrystalline CuO – ZnO nanocomposite. These results are matching well the previously reported works [48].

XPS measurements were investigated for further explanation about the structure in terms of bonding characteristics, oxidation states and purity. The XPS spectra of CuO-ZnO nanoparticles were demonstrated in Fig. 6. It is clear from the full survey scan spectrum of the prepared sample that there were four detected atoms attributed to Zn

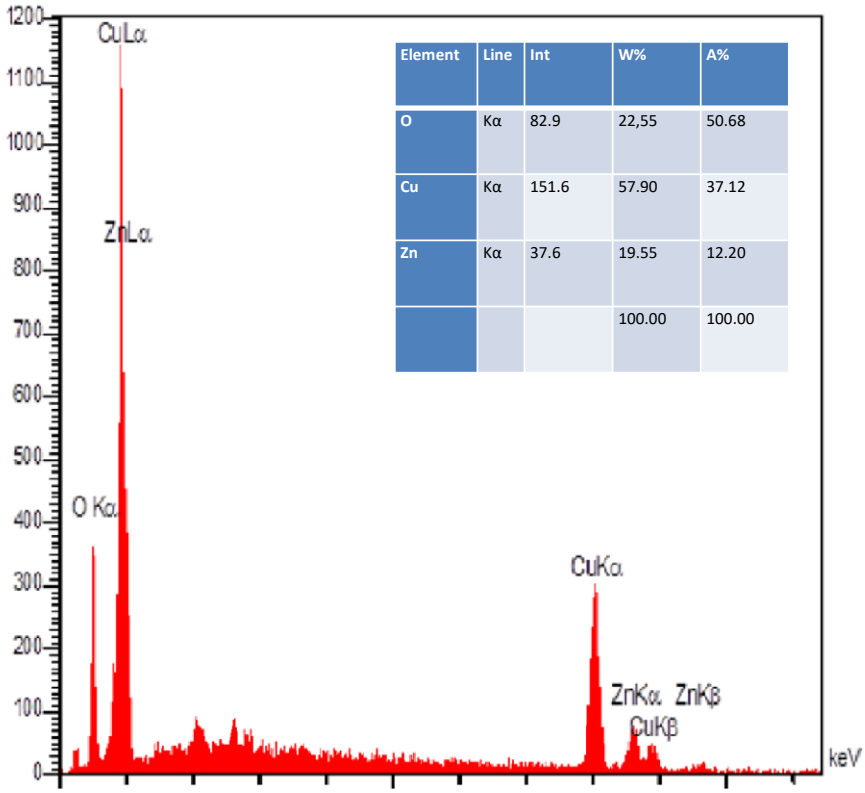

Element	Line	Int	W%	A%
O	Kα	82.9	22,55	50.68
Cu	Kα	151.6	57.90	37.12
Zn	Kα	37.6	19.55	12.20
			100.00	100.00

Fig. 3. EDX spectra of prepared CuO-ZnO nanostructures.

2p, Cu 2p, O 1s and C 1s as shown in Fig. 6 (a). The C 1s peak could be attributed to the hydrocarbon impurity inside the XPS instrument, nevertheless, the biding energies were standardized according to the signal from adventitious carbon (284.5 eV). It is also observed that the spectrum is free from other peaks related to impurities which indicating that the prepared sample was a highly pure composite. To evaluate the chemical nature of carbon atoms in the prepared sample, the narrow scan XPS spectra of the C 1s region as illustrated in Fig. 6 (b). Two peaks related to carbon atoms were detected at 284.5 eV and 286.9 eV which were assigned to C-C and C-O, respectively [49, 50].

The high resolution of the Cu 2p core-level XPS spectrum is shown in Fig. 6 (c). Four 962 eV, 952.5 eV, 942.5 eV and 932.45 eV were attributed to shackup satellite, Cu 2p1/2, shackup satellite and Cu 2p3/2, respectively. Out of these, there are two major detected peaks that correspond to Cu 2p, namely Cu 2p 1/2 and Cu 2p 3/2 centered at 952.5 eV and 932.45 eV matching well with previously reported values [51, 52]. The existence of two Cu 2p peaks indicated the presence of two types of Cu ions. When Cu 2p core level spectrum displays Cu 2p 1/2 at 952.5 eV indicated that CuO owing the Cu^{2+} (d^9) ground state configuration [53]. This can be ascribed to the existence of O species on the surface of the sample [54]. Meanwhile, the asymmetrical peak of Cu 2p3/2 at 932.45 eV corresponds to Cu^{1+} (d^{10}) ion [55]. In another hand, the two shackup satellite peaks centered at 962.1 eV and 942.5 eV originated from the electron transitions. During the photoejection of a core electron, the valance band electron excited to the higher unoccupied bands. This transition leads to reduce the kinetic energy of the photoejected electron lowest than the energy of another molecule electrons in the same core orbital [56].

It is noticed that the fitting of the asymmetric O 1s contains three peaks as depicted in Fig. 6 (d). These three peaks located at 533 eV, 531 eV and 529 eV correspond to O chemisorbed, O in lattice and MO, respectively. The small peak at 533 eV. The other peak at 531 eV corresponds to adsorbed CO_2 [57]. The strongest peak at 529.7 eV corresponds to CuO according to (CAS No 1317-38-0).

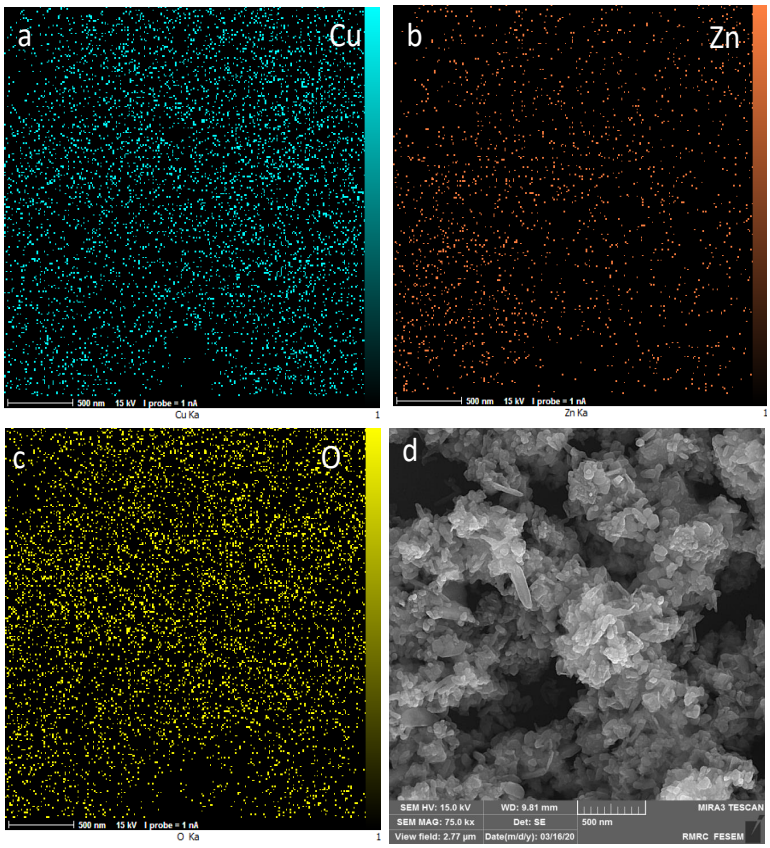

Fig. 4. EDX spectra of the prepared CuO-ZnO nanostructures in which (a) Cu, (b) Zn, (c) O and (d) the corresponding FESEM image.

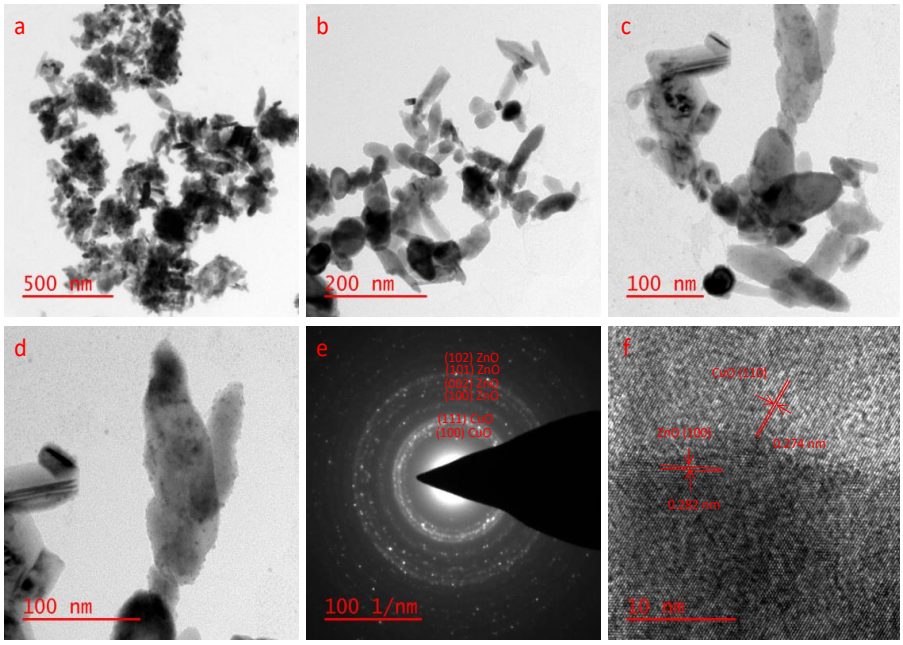

Fig. 5. TEM spectra of the prepared CuO-ZnO nanostructures in which (a) TEM low magnification, (b) , (c) and (d) TEM with high magnification, (e) SAED (f) HRTEM.

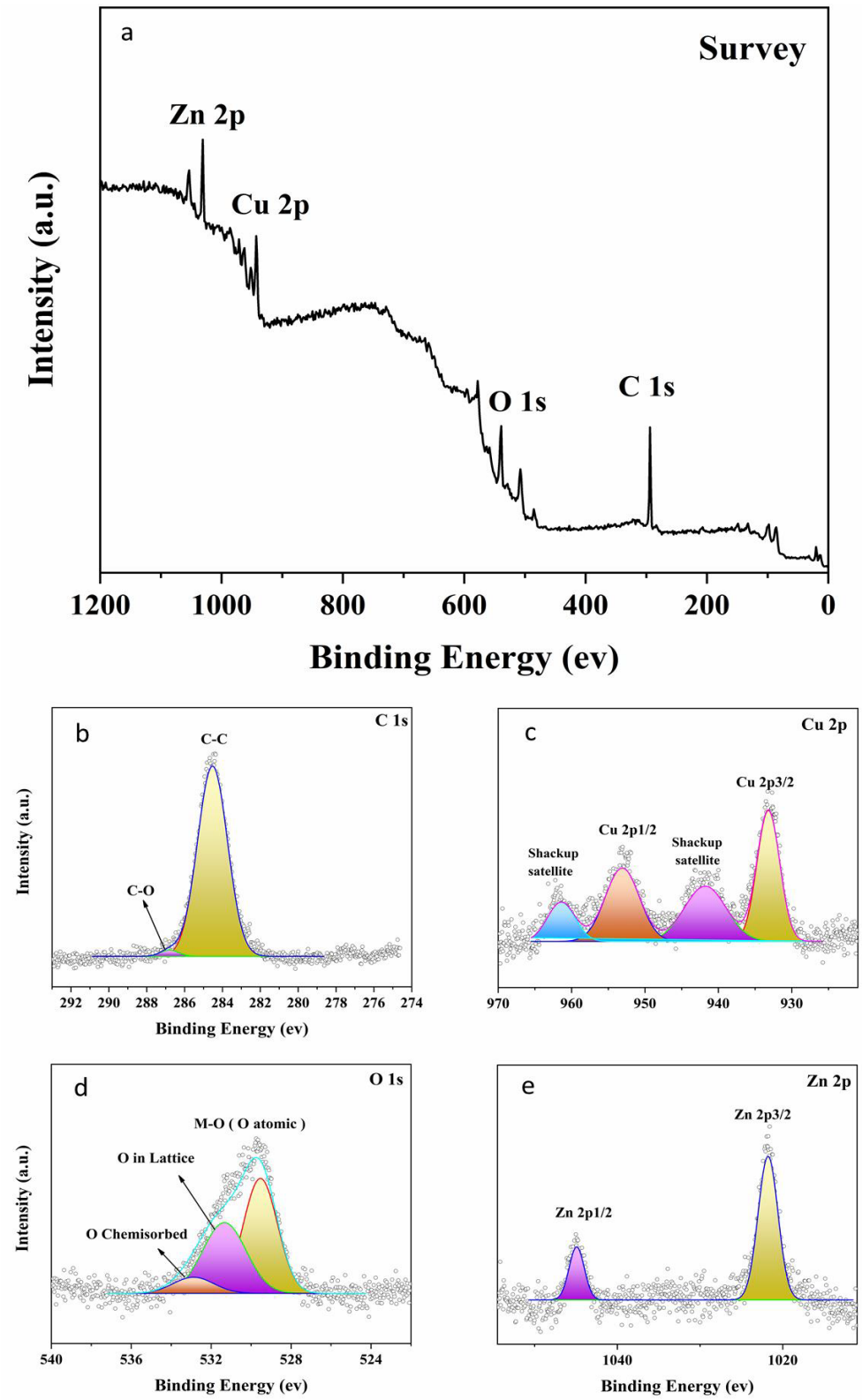

Fig. 6. XPS spectra of sample CuO-ZnO (a) survey spectra (b) C 1s spectra (c) Cu 2p spectra (d) O 1s spectra and (e) Zn 2p spectra.

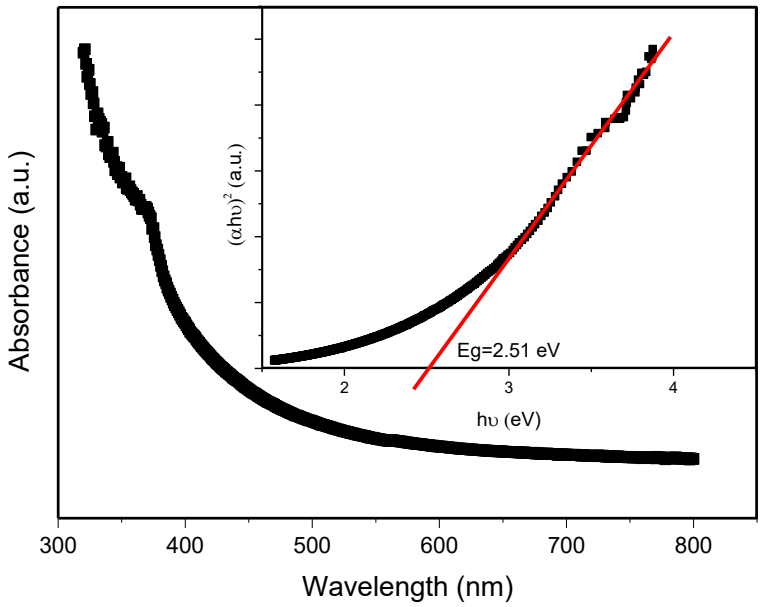

Fig. 7. The UV/Vis spectrum of CuO-ZnO.

Nevertheless, in Fig. 6 (e), it is noticed that there are two main well-characterized and separated peaks. These peaks are centered at a binding energy of 1021.9 eV and 1044.5 eV which corresponds to 2p3/2 and 2p1/2, respectively (CAS No 1314-13-2) [58, 59]. The large binding energy separation around 23 eV indicating the presence of Zn(II) [60].

To investigate the optical properties, UV/Vis spectrum of CuO-ZnO was studied as shown in Fig. 7. The spectrum revealed the presence of a shoulder at 372.4 nm related to intrinsic band gap of ZnO owing to the transition of electrons from the valance band to the conductance band (O^{2p} to Zn^{3d}). The insight figure showed the energy gap of the CuO-ZnO which is equal to Eg=2.51 eV. This variation in band gap is extremely successful approach to decelerate the electron–hole pair's

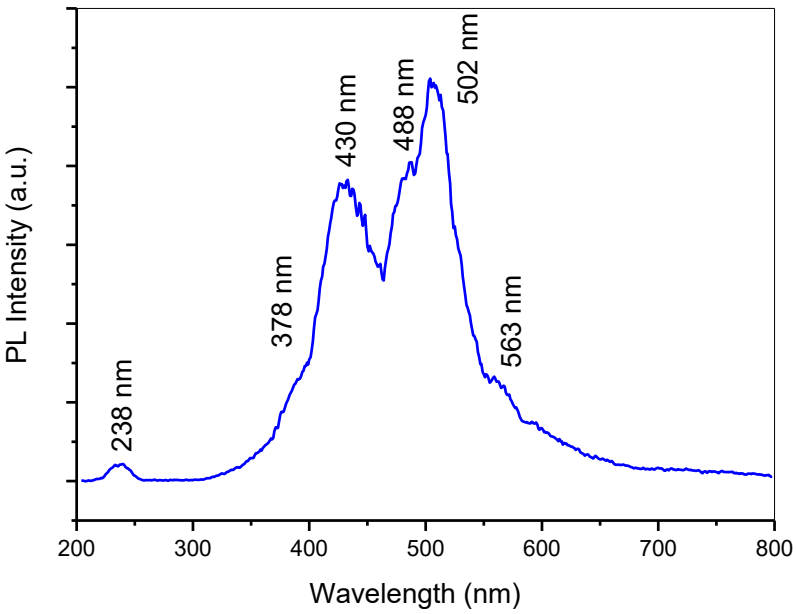

Fig. 8. PL spectra of sample CuO-ZnO.

recombination. The unique features of the new coupled structure permit to control their performance. Comparing to previous work the energy gap of CuO – ZnO value depends on several parameters such as shape, size and the ratio of ZnO to CuO. As example 20 nm spherical CuO – ZnO exhibited energy gap varied from 3.07 to 3.22 eV [61]. Another reported work revealed that the energy gap of nanorods CuO-ZnO is decreased from 2.6 to 2.4 as the Cu amount increased [62]. Meanwhile, other researchers described the energy gap of CuO – ZnO nanorods as 1.5 eV with ham at 3.2 eV related to ZnO [63].

The effects of doping CuO with Zn ions in terms of intrinsic and extrinsic defects were investigated using photoluminescence (PL) in the wavelength range between 200 – 800 nm as shown in Fig. 8. The spectra vouchsafed emission peaks at 238 nm, 430 nm, 488 nm and 502 nm. The shoulder at 378 nm is attributed to exciton transitions in the UV region relates to the band energy 3.28 eV [64]. As well, the peak at 430 nm followed the energy band of 2.45 eV originated from defects caused by oxygen vacancies [65]. The small PL peaks in the range between 450 to 475 nm could be attributed to the intrinsic defects of surface states in CuO [66]. As well as, the two peaks at 488 nm and 502 nm at the energy of 2.88 eV and 2.47 eV, respectively are originated from CuO original [67-69]. The orange-red emission at 563 nm is attributed to ZnO [70].

CONCLUSION

In the current work, binary system of CuO-ZnO nanostructures was prepared using hydrothermal method. XRD measurements revealed that the CuO-ZnO nanostructures displayed the presence of monoclinic CuO and hexagonal phase ZnO. The SEM micrographs revealed that the morphology of the prepared sample was nanorods. The XPS spectrum revealed that the papered sample was free from other impurities. The HRTEM confirmed the existence of quantum dots coating the nanorods. We have demonstrated that the CuO-ZnO binary system is a promising candidate for several applications.

CONFLICT OF INTEREST

The authors declare that there is no conflict of interests regarding the publication of this manuscript.

REFERENCES

1. Alosfur FKM, Ridha NJ. Synthesis and characterization of ZnO/SnO_2 nanorods core–shell arrays for high performance gas sensors. Appl Phys A. 2021;127(3):1-11.
2. Xu J, Liu C, Wu Z. Direct electrochemistry and enhanced electrocatalytic activity of hemoglobin entrapped in graphene and ZnO nanosphere composite film. Microchimica Acta. 2011;172(3-4):425-430.
3. Maged A, Madian AH, Raafat AI, Ali AE-H, editors. Cole-Cole Modelling of Reduced Graphene Oxide Decorated CuO Nano-Spheres Based Waterproof Conductive Ink for Flexible Electrodes. 2021 38th National Radio Science Conference (NRSC); 2021: IEEE.
4. Li J, Cheng K, Xu P, Lee C. Lateral semiconductor nanotube with hexagonal shape. Google Patents; 2020.
5. Hou L, Zhang C, Li L, Du C, Li X, Kang X-F, et al. CO gas sensors based on p-type CuO nanotubes and CuO nanocubes: Morphology and surface structure effects on the sensing performance. Talanta. 2018;188:41-49.
6. Wang L, Borrelli M, Simmchen J. Self-asymmetric yolk-shell photocatalytic ZnO micromotor. ChemPhotoChem.
7. Prajapati K, Johns B, Bandopadhyay K, Silva SRP, Mitra J. Interaction of ZnO nanorods with plasmonic metal nanoparticles and semiconductor quantum dots. The Journal of Chemical Physics. 2020;152(6):064704.
8. Ridha NJ, Jumali MHH, Umar AA, Alosfur F. Defects-controlled ZnO nanorods with high aspect ratio for ethanol detection. Int J Electrochem Sci. 2013;8:4583-4594.
9. Chen X, Zhao S, Zhou P, Cui B, Liu W, Wei D, et al. Room-temperature NO_2 sensing properties and mechanism of CuO nanorods with Au functionalization. Sensors Actuators B: Chem. 2021;328:129070.
10. Umran NM, Rashed HA, Alosfur FKM, Ridha NJ, editors. Effect of substitution (Al and P) atoms in ZnO nanosheet on structural and electronic properties. Journal of Physics: Conference Series; 2018: IOP Publishing.
11. Ouda AA, Alosfur FKM, Ridha NJ, Abud SH, Umran NM, Al-aaraji HH, et al., editors. Facile method to synthesis of anatase TiO_2 nanorods. Journal of Physics: Conference Series; 2018: IOP Publishing.
12. Alosfur FKM, Jumali MH, Radiman S, Ridha NJ, Umar AA, editors. Visible light photocatalytic activity of TiO_2/MWCNTs nanocomposite prepared using modified microwave technique. 2013 Seventh International Conference on Sensing Technology (ICST); 2013: IEEE.
13. Alosfur FKM, Ouda AA, Ridha NJ, Abud SH, editors. Structure and optical properties of TiO_2 nanorods prepared using polyol solvothermal method. AIP Conf Proc; 2019: AIP Publishing LLC.
14. Chandraker SK, Lal M, Ghosh MK, Tiwari V, Ghorai TK, Shukla R. Green synthesis of copper nanoparticles using leaf extract of Ageratum houstonianum Mill. and study of their photocatalytic and antibacterial activities. Nano Express. 2020.
15. Tanaka T, Saito K, Guo Q, Yu KM, Walukiewicz W, editors. Intermediate band solar cells based on highly mismatched II-VI oxide semiconductors. Oxide-based Materials and Devices XI; 2020: International Society for Optics and Photonics.
16. Radhi MM, Alosfur FKM, Ridha NJ. Voltammetric characterization of grafted polymer modified with ZnO nanoparticles on glassy carbon electrode. Russ J Electrochem. 2018;54(1):27-32.
17. Ridha NJ, Alosfur FKM, Jumali MHH, Radiman S. Dimensional effect of ZnO nanorods on gas-sensing performance. J Phys

D: Appl Phys. 2018;51(43):435101.
18. Jumali MHH, Alosfur FKM, Radiman S, Ridha NJ, Yarmo MA, Umar AA. Rapid synthesis of TiO_2/MWCNTs nanocatalyst with enhanced photocatalytic activity using modified microwave technique. Mater Sci Semicond Process. 2014;25:207-210.
19. Alosfur FKM, Ouda AA, Ridha NJ, Abud SH. High photocatalytic activity of TiO_2 nanorods prepared by simple method. Materials Research Express. 2019;6(6):065028.
20. Alosfur F, Jumali MH, Radiman S, Ridha NJ, Yarmo MA, Umar AA. Visible light-responsive TiO_2 coated MWCNTs as a hybrid nanocatalysts. Int J Electrochem Sci. 2013;8:2977-2982.
21. Alosfur FKM, Ridha NJ, Jumali MHH, Radiman S. One-step formation of TiO_2 hollow spheres via a facile microwave-assisted process for photocatalytic activity. Nanotechnology. 2018;29(14):145707.
22. Alosfur FKM, Jumali MHH, Radiman S, Ridha NJ, Yarmo MA, Umar AA. Modified microwave method for the synthesis of visible light-responsive TiO_2/MWCNTs nanocatalysts. Nanoscale research letters. 2013;8(1):346.
23. Ridha NJ, Alosfur FK, Kadhim HBA, Ahmed LM. Synthesis of Ag decorated TiO_2 nanoneedles for photocatalytic degradation of methylene blue dye. Materials Research Express. 2021.
24. Liu B, Chen D, Lu H, Tao T, Zhuang Z, Shao Z, et al. Hybrid Light Emitters and UV Solar-Blind Avalanche Photodiodes based on III-Nitride Semiconductors. Adv Mater. 2020;32(27):1904354.
25. Alkhayatt AHO, Jaafer MD, Al Alak HHA, Ali AH. Characterization of CuO/n–Si pn junction synthesized by successive ionic layer adsorption and reaction method. Optical and Quantum Electronics. 2019;51(7):1-13.
26. Mallick P, Sahu S. Structure, microstructure and optical absorption analysis of CuO nanoparticles synthesized by sol-gel route. Nanosci Nanotechnol. 2012;2(3):71-74.
27. Dar M, Kim Y, Kim W, Sohn J, Shin H. Structural and magnetic properties of CuO nanoneedles synthesized by hydrothermal method. Appl Surf Sci. 2008;254(22):7477-7481.
28. Lugo-Ruelas M, Amézaga-Madrid P, Esquivel-Pereyra O, Antúnez-Flores W, Pizá-Ruiz P, Ornelas-Gutiérrez C, et al. Synthesis, microstructural characterization and optical properties of CuO nanorods and nanowires obtained by aerosol assisted CVD. J Alloys Compd. 2015;643:S46-S50.
29. Chen A, Long H, Li X, Li Y, Yang G, Lu P. Controlled growth and characteristics of single-phase Cu_2O and CuO films by pulsed laser deposition. Vacuum. 2009;83(6):927-930.
30. Wang Y-t, Zhang X-t, Xu J-b, Shen Y, Wang C-a, Li F-w, et al. Fabrication and characterization of Al–CuO nanocomposites prepared by sol-gel method. Defence Technology. 2021;17(4):1307-1312.
31. Yao W, Li F-L, Li H-X, Lang J-P. Fabrication of hollow Cu_2O@CuO-supported Au–Pd alloy nanoparticles with high catalytic activity through the galvanic replacement reaction. Journal of Materials Chemistry A. 2015;3(8):4578-4585.
32. Zhang X, Yang Y, Que W, Du Y. Synthesis of high quality CuO nanoflakes and CuO–Au nanohybrids for superior visible light photocatalytic behavior. RSC advances. 2016;6(85):81607-81613.
33. Qian J, Hu Q, Hou X, Qian F, Dong L, Li B. Study of different Ti/Zr ratios on the physicochemical properties and catalytic activities for CuO/Ti–Zr–O composites. Ind Eng Chem Res. 2018;57(38):12792-12800.
34. Huang K, Li Z, Xu Q, Liu H, Li H, Wang Y. Lithiophilic cuo nanoflowers on Ti-mesh inducing lithium lateral plating enabling stable lithium-metal anodes with ultrahigh rates and ultralong cycle life. Advanced Energy Materials. 2019;9(29):1900853.
35. Zhang J, Ma S, Wang B, Pei S. Hydrothermal synthesis of SnO_2-CuO composite nanoparticles as a fast-response ethanol gas sensor. J Alloys Compd. 2021;886:161299.
36. Yousefi A, Nezamzadeh-Ejhieh A, Mirmohammadi M. The coupled CuO-SnO_2 catalyst: Characterization and the photodegradation kinetics towards phenazopyridine. Environmental Technology & Innovation. 2021;22:101496.
37. Asadi A, Alarifi IM, Foong LK. An experimental study on characterization, stability and dynamic viscosity of CuO-TiO_2/water hybrid nanofluid. J Mol Liq. 2020;307:112987.
38. Kadhim HBA, Ridha NJ, Alosfur FKM, Umran NM, Madlol R, Tahir KJ, et al., editors. Ablation of ZnO in liquid by Nanosecond Laser. Journal of Physics: Conference Series; 2018: IOP Publishing.
39. Ridha NJ, Kadhim HBA, Alosfur FKM, Abood LH, Madlol R, editors. Synthesis ZnO nanoparticles by LAL method using different energies of Nd-YAG laser. AIP Conf Proc; 2019: AIP Publishing LLC.
40. Thaweesaeng N, Supankit S, Techidheera W, Pecharapa W. Structure properties of as-synthesized Cu-doped ZnO nanopowder synthesized by co-precipitation method. Energy Procedia. 2013;34:682-688.
41. Phiwdang K, Suphankij S, Mekprasart W, Pecharapa W. Synthesis of CuO nanoparticles by precipitation method using different precursors. Energy procedia. 2013;34:740-745.
42. Phoohinkong W, Foophow T, Pecharapa W. Synthesis and characterization of copper zinc oxide nanoparticles obtained via metathesis process. Advances in Natural Sciences: Nanoscience and Nanotechnology. 2017;8(3):035003.
43. Pinthong P, Klongklaew P, Praserthdam P, Panpranot J. Effect of the Nanostructured Zn/Cu Electrocatalyst Morphology on the Electrochemical Reduction of CO_2 to Value-Added Chemicals. Nanomaterials. 2021;11(7):1671.
44. Fernández Y, Menéndez J, Arenillas A, Fuente E, Peng J, Zhang Z, et al. Microwave-assisted synthesis of CuO/ZnO and CuO/ZnO/Al_2O_3 precursors using urea hydrolysis. Solid State Ionics. 2009;180(26-27):1372-1378.
45. Munir T, Mahmood A, Ahmad N, Atif M, Alimgeer K, Fatehmulla A, et al. Structural, electrical and optical properties of $Zn_{1-x}Cu_xO$ (x= 0.00–0.09) nanoparticles. Journal of King Saud University-Science. 2021;33(2):101330.
46. Kumar JP, Prasad G, Ramacharyulu P, Garg P, Ganesan K. Mesoporous CuO–ZnO binary metal oxide nanocomposite for decontamination of sulfur mustard. Materials Chemistry and Physics. 2013;142(2-3):484-490.
47. Sanmugam A, Vikraman D, Karuppasamy K, Lee JY, Kim H-S. Evaluation of the corrosion resistance properties of electroplated chitosan-$Zn_{1-x}Cu_xO$ composite thin films. Nanomaterials. 2017;7(12):432.
48. Malwal D, Gopinath P. CuO-ZnO Nanosheets with p–n Heterojunction for Enhanced Visible Light Mediated Photocatalytic Activity. ChemistrySelect. 2017;2(17):4866-4873.
49. Zhu K, Jin C, Klencsár Z, Ganeshraja AS, Wang J. Cobalt-iron oxide, alloy and nitride: synthesis, characterization and application in catalytic peroxymonosulfate activation for

orange II degradation. Catalysts. 2017;7(5):138.
50. Saha A, Basiruddin S, Ray SC, Roy S, Jana NR. Functionalized graphene and graphene oxide solution via polyacrylate coating. Nanoscale. 2010;2(12):2777-2782.
51. Sarkar S, Basak D. Defect controlled ultra high ultraviolet photocurrent gain in Cu-doped ZnO nanorod arrays: De-trapping yield. Appl Phys Lett. 2013;103(4):041112.
52. Meng L, Zhao H. Low-temperature complete removal of toluene over highly active nanoparticles CuO-TiO_2 synthesized via flame spray pyrolysis. Applied Catalysis B: Environmental. 2020;264:118427.
53. Sharma K, Raizada P, Hosseini-Bandegharaei A, Thakur P, Kumar R, Thakur VK, et al. Fabrication of efficient CuO/graphitic carbon nitride based heterogeneous photo-Fenton like catalyst for degradation of 2, 4 dimethyl phenol. Process Saf Environ Prot. 2020;142:63-75.
54. Hu L, Shi L, Hong H, Li M, Bao Q, Tang J, et al. Catalytic epoxidation of stilbene with FePt@ Cu nanowires and molecular oxygen. Chem Commun. 2010;46(45):8591-8593.
55. Wang Z, Xiao W, Tian M, Qin N, Shi H, Zhang X, et al. Effects of Copper Dopants on the Magnetic Property of Lightly Cu-Doped ZnO Nanocrystals. Nanomaterials. 2020;10(8):1578.
56. Brisk MA, Baker A. Shake-up satellites in X-ray photoelectron spectroscopy. J Electron Spectrosc Relat Phenom. 1975;7(3):197-213.
57. Hagman B, Posada-Borbón A, Schaefer A, Shipilin M, Zhang C, MERTE LR, et al. Steps control the dissociation of CO_2 on Cu (100). Journal of the American Chemical Society. 2018;140(40):12974-12979.
58. Wu Y, Lin Y, Xu J. Synthesis of Ag–Ho, Ag–Sm, Ag–Zn, Ag–Cu, Ag–Cs, Ag–Zr, Ag–Er, Ag–Y and Ag–Co metal organic nanoparticles for UV-Vis-NIR wide-range bio-tissue imaging. Photochemical & Photobiological Sciences. 2019;18(5):1081-1091.
59. Zhang F, Li Y-H, Qi M-Y, Tang Z-R, Xu Y-J. Boosting the activity and stability of Ag-Cu_2O/ZnO nanorods for photocatalytic CO2 reduction. Applied Catalysis B: Environmental. 2020;268:118380.
60. Kim K, Razzaq A, Sorcar S, Park Y, Grimes CA, In S-I. Hybrid mesoporous Cu_2ZnSnS_4 (CZTS)–TiO_2 photocatalyst for efficient photocatalytic conversion of CO_2 into CH 4 under solar irradiation. RSC Advances. 2016;6(45):38964-38971.
61. Liu X, Liu H, Zhang W, Li X, Fang N, Wang X, et al. Facile synthesis and photocatalytic activity of bi-phase dispersible Cu-ZnO hybrid nanoparticles. Nanoscale research letters. 2015;10(1):1-9.
62. Ma C, Liu Z, Tong Z, Han C, Cai Q. Plasmonic Ag nanoparticles and p-type CuO-modified ZnO nanorods for efficient photoelectrochemical water splitting. Appl Phys A. 2019;125(7):1-9.
63. Shaislamov U, Krishnamoorthy K, Kim SJ, Abidov A, Allabergenov B, Kim S, et al. Highly stable hierarchical p-CuO/ZnO nanorod/nanobranch photoelectrode for efficient solar energy conversion. Int J Hydrogen Energy. 2016;41(4):2253-2262.
64. Bhuvaneshwari S, Gopalakrishnan N. Hydrothermally synthesized Copper Oxide (CuO) superstructures for ammonia sensing. Journal of colloid and interface science. 2016;480:76-84.
65. Albadarin NA, Takriff MS, Tan ST, Shahahmadi SA, Minggu LJ, Kadhum AAH, et al. Tunable morphology and band gap alteration of CuO-ZnO nanostructures based photocathode for solar photoelectrochemical cells. Materials Research Express. 2020;7(12):125010.
66. Goyal CP, Goyal D, K Rajan S, Ramgir NS, Shimura Y, Navaneethan M, et al. Effect of Zn Doping in CuO Octahedral Crystals towards Structural, Optical, and Gas Sensing Properties. Crystals. 2020;10(3):188.
67. Yadav I, Ahlawat DS. Effect of dopant concentration on structural and optical properties of $Cd_{0.7}Zn_{0.3}S$ semiconducting nanocrystals. Materials Science and Engineering: B. 2020;252:114450.
68. Huang C-Y, Chatterjee A, Liu S, Wu S, Cheng C-L. Photoluminescence properties of a single tapered CuO nanowire. Appl Surf Sci. 2010;256(11):3688-3692.
69. Shkir M, Khan Z, Anis M, Shaikh S, AlFaify S. A comprehensive study of opto-electrical and nonlinear properties of Cu@CdS thin films for optoelectronics. Chinese Journal of Physics. 2020;63:51-62.
70. Biroju RK, Giri P. Strong visible and near infrared photoluminescence from ZnO nanorods/nanowires grown on single layer graphene studied using sub-band gap excitation. J Appl Phys. 2017;122(4):044302.